A Resampling of Calibration Images for a Multi-Coil Separation of Parallel Encoded Complex-valued Slices in fMRI

Mary C. Kociuba[a], Andrew S. Nencka[b], and Daniel B. Rowe[b,c*]

[a] Departments of Pediatrics and Bioengineering
University of Washington, Seattle, WA USA
[b] Department of Mathematics, Statistics, and Computer Science
Marquette University, Milwaukee WI, USA
[c] Department of Biophysics
Medical College of Wisconsin, Milwaukee WI, USA

*Corresponding Author
Daniel B. Rowe, Ph.D.
Department of Mathematics, Statistics, and Computer Science
Marquette University, Milwaukee, Wisconsin, USA
Email: daniel.rowe@marquette.edu
Phone: 1-414-288-5228
FAX: 1-414-288-5472

ABSTRACT

Increasing temporal resolution while mitigating signal leakage has been a challenge of simultaneous multi-slice (SMS) imaging in functional magnetic resonance imaging. The Multi-Coil Separation of Parallel Encoded Complex-valued Slices (mSPECS) reconstruction method minimizes residual signal artifacts from time-series un-aliasing, and preserves the blood oxygen level dependent (BOLD) signal in fMRI studies. In the mSPECS reconstruction model, multiple slices are simultaneously excited with a Hadamard multiband pulse sequence. With Hadamard encoded acquisitions, the separated images have increased sensitivity with no net reduction in the scan duration. The mSPECS reconstruction method has incorporated the spatial information from a phased array of receiver coils, combined with a bootstrap sampling and artificial Hadamard aliasing of calibration images, to separate the fMRI time-series with a visual task in a least squares estimation. Faster brain function observation is dynamically achieved post data acquisition in a visual task fMRI experiment. The aliased slices are effectively separated, and functional activation is detected in the visual cortex. The mSPECS model has combined calibration images with intrinsic orthogonal properties of Hadamard encoding, into a un-aliasing estimator to achieve separated images of fMRI time-series.

Keywords: fMRI; simultaneous multi-slice (SMS); multiband; Hadamard Encoding; leakage

1. Introduction

Echo planar imaging methods are commonly used to measure blood oxygen level dependent (BOLD) contrast in functional magnetic resonance imaging (fMRI) studies, where the magnetization of an individual slice is flipped by a radiofrequency (RF) pulse and reconstructed from a single complex-valued *k*-space readout. Standard in-plane parallel MRI acceleration methods speed-up scan time from subsampling the *k*-space readout through omitting rows of the spatial frequency measurements at each receiver coil (1-3). During Fourier image reconstruction, the missing lines in the *k*-space readout are interpolated with additional localized spatial information derived from fully sampled coil sensitivity profiles. In-plane parallel imaging methods achieve an acceleration factor of 2 or 3, with a signal-to-noise ratio (SNR) penalty relative to the number of skipped rows and the coil dependent geometry factor. Temporal resolution is also constrained by the long echo time (TE) required to achieve BOLD contrast in the reconstructed images. Simultaneous multi-slice (SMS) is a rapidly advancing imaging technique which substantially speeds up scan time compared to traditional in-plane parallel imaging methods, with a marginal SNR loss in the reconstructed images. SMS-fMRI imaging techniques overcome the TE limitation by simultaneously exciting multiple slices, rather than increasing the number of *k*-space lines skipped, to achieve higher acceleration rates. With SMS methods, the TR is effectively shortened as less time is required to acquire the slice images, although without full signal recovery there is a reduction of the SNR. A speed-up of the acquisition allows for a higher sampling rate of time points, increases the confidence of the activation statistics in the fMRI time-series analysis, and shortens the TR enough for neural hemodynamics to be modeled with full brain coverage.

An early SMS imaging strategy used receiver coil sensitivity profiles to separate the individual slices (4). More recently, studies combine coil sensitivities along with the use of incremental shifts in either the frequency or the phase encoding directions (5). The shifts achieve a larger differential among the coil sensitivity profiles and aliased voxel values, improving the stability of the separation matrix. Inter-slice aliasing artifacts still limit SMS imaging methods, and efforts have been made to characterize and alleviate signal leakage in separated slices in the context of optimized SMS acquisition and reconstruction methods (5-7). Despite the advancements in SMS imaging, as acceleration factors increase, there is not always sufficient information for identifying the BOLD signal, resulting in signal leakage in the previously aliased

voxels (8). SMS inter-slice signal leakage is generally non-uniform across previously aliased slices, which makes it difficult to identify the source of the image distortion, and an unsatisfactory slice separation may appear as brain connectivity during the fMRI analysis.

Hadamard encoding is another early SMS method, where the RF pulse modulates the phase magnetization in each excited slice (9,10). With a unique phase encoding imparted to each slice in a cyclical pattern throughout the time-series, individual slices are resolved through solving a system of linear equations with sequential acquisitions. The original reconstruction of Hadamard encoded images offers no increase in the acceleration factor, rather a means to uniquely tag aliased slices through a time-series, with an improvement in the SNR. The mSPECS reconstruction method outlined in this manuscript proposes a Hadamard encoded image acquisition, with a random sampling of calibration images, to separate slice images. Fully sampled complex-valued calibration images are bootstrap sampled and artificially aliased, to separate the aliased time-series with increased acceleration. The bootstrapping algorithm at each time point induces negligible correlation between previously aliased voxels, so inter-slice signal leakage is avoided and the BOLD signal is preserved in the un-aliased fMRI time-series, and faster observation of brain function is achieved. Without the mitigation of inter-slice signal leakage in SMS-fMRI acquisition and reconstructions, brain networks will not be appropriately modeled in full volume studies. Previous studies have also shown that complex-valued time-series models, over magnitude-only models, offer improved fMRI activation statistics (11-15) and slice separation in SMS reconstruction (16,17).

2. Theory

The Multi-coil Separation of Parallel Encoded Complex-valued Slices (mSPECS) reconstruction method is a one-step process of slice image separation and coil image combination. In mSPECS, H, as constructed with the Sylvester method (18), is the Hadamard aliasing matrix for an experiment with n_S aliased slice images, and is of dimension $n_S \times n_S$. For example, an acquisition of $n_S = 4$ aliased slice images uses the orthogonal Hadamard aliasing matrix,

$$H = \begin{bmatrix} 1 & 1 & 1 & 1 \\ 1 & -1 & 1 & -1 \\ 1 & 1 & -1 & -1 \\ 1 & -1 & -1 & 1 \end{bmatrix}.$$

Row δ and column z of H is denoted $H_{\delta,z}$ for the Hadamard aliasing pattern δ, corresponding to a given time repetition (TR), for slice z. The parameter n_S corresponds to the number of aliased slice images per packet, or the multiband (MB) factor. The term packet refers to the number of aliased slice groups, i.e. n_S = 4 for 2 packets is a total of 8 slice acquisition bandwidth of ±250 images acquired with MB 4. Fig. 1 is a diagram of the slice profiles for 2 aliased slice images in 2 packets acquired over 2 TRs, where the first TR corresponds to the [+ +] Hadamard excitation, the second TR corresponds to the [+ -] Hadamard excitation, and then the pattern will repeat for the subsequent TRs.

*** Fig. 1 appears near here***

The remaining parts of the Theory section is divided into three parts, first is a description of a single aliased voxel value from a Hadamard encoded acquisition measured at multiple coils, second is a description of the bootstrap sampling and the artificial aliasing of the voxel values from the calibration slice images measured at multiple coils, and third is a description of the separation of the aliased voxel values with a discussion on the correlation of the previously aliased voxel values.

2.1 A single aliased voxel

In one packet, a single aliased voxel, $a_{j,\delta}$, in the same (x,y) voxel location across n_S slices, with the Hadamard encode δ, measured at coil j, in image space is written as the summation

$$a_{j,\delta} = \sum_{s=1}^{n_S} H_{\delta,s} S_{j,s} \beta_s + \varepsilon_j. \quad [1]$$

The Hadamard coefficient $H_{\delta,z}$ will be either 1 or -1, and the 2×1 vector $a_{j,\delta}$ is the real and imaginary parts of an aliased voxel acquired with the Hadamard aliasing pattern δ measured at coil j. In Eq. [1], $a_{j,\delta}$ is written as the sum of the 2×1 vector β_z, the real and imaginary parts of the true voxel value in slice z, weighted by the 2×2 matrix of real and imaginary coil sensitivities at coil j. The parameter $S_{j,z}$ is the real and imaginary coil sensitivities that correspond to the same (x,y) voxel location as β_z for slice z at coil j, in a skew symmetric matrix, $S_{j,z} = [S_R,-S_I;S_I,S_R]_{j,z}$. The 2×1 vector $\varepsilon_j=(\varepsilon_{jR},\varepsilon_{jI})'$ is the measurement error with real and imaginary parts at coil j with a mean of $E(\varepsilon_j) = 0$ and covariance of $cov(\varepsilon_j) = \sigma^2 I_2$, where I_2 is a 2×2 identity matrix.

To separate the n_S aliased voxels at a single voxel location, the goal is to estimate β, the true $2n_S$ real and imaginary voxel values from one packet. The number of sequential time-points, n_α, where n_α is an integer between 1 and n_S, is the number of sequential TRs in the Hadamard encoded acquisition included in the separation of a single separated aliased voxel at one time point. If the data is acquired in packets of n_S aliased slices, the net acceleration of the slice image time-series acquisition is

$A=n_S/n_\alpha$.

The measured aliased voxel in Eq. [1] is generalized across n_C coils for n_S aliased slices with n_α sequential time-points included in the separation, as

$$a = X_A\beta+\varepsilon. \quad [2]$$

In Eq. [2], a and ε are of dimension $2n_Cn_\alpha\times1$, and the error vector, ε, has the mean of

$E(\varepsilon) = 0$,

and a covariance of

$$\text{cov}(\varepsilon) =\sigma^2 I_{2n_Cn_\alpha}, \quad [3]$$

X_A is of dimension $2n_Cn_\alpha\times2n_S$, and β is of dimension $2n_S\times1$. For the δ^{th} aliasing pattern, the aliasing matrix $(X_A)_\delta$ of dimension $2n_C\times2n_S$ is constructed by multiplying the Hadamard coefficients with the coil sensitivities,

$$(X_A)_\delta=\left[H_{\delta,1}\begin{pmatrix} S_{1,1} \\ \vdots \\ S_{n_C,1}\end{pmatrix},\dots,H_{\delta,n_S}\begin{pmatrix} S_{1,n_S} \\ \vdots \\ S_{n_C,n_S}\end{pmatrix}\right].$$

This is generalized to X_A, of dimension $2n_\alpha n_C\times2n_S$, for the incorporation of n_α sequential TRs in the aliased voxel separation,

$$X_A = [(X_A)_1,\dots,(X_A)_{n_\alpha}]'. \quad [4]$$

Similar to previous efforts to disentangle simultaneously excited slices with coil sensitivities (4), although with an additional phase manipulation (9,10), the $2n_S\times1$ vector of separated voxel values, $\hat{\beta}$, can be estimated,

$\hat{\beta}=(X'_A X_A)^{-1} X'_A a$,

with a covariance between the previously aliased voxels across the n_S slices,

$$\text{cov}(\hat{\beta})=\sigma^2 (X_A'X_A)^{-1}. \quad [5]$$

To reduce the covariance between previously aliased voxels, and thus minimize correlation induced from the aliased voxel separation process, the mSPECS method combines the coil and

phase encoding with calibration images used in the least squares estimation. The novelty of the mSPECS reconstruction is a bootstrapping sampling and artificial aliasing of calibration voxel values, from a separate acquisition of fully-sampled slice image time-series, that are artificially aliased in the remaining Hadamard pattern for a given TR. This mechanism of incorporating calibration slice images in the SMS-fMRI reconstruction, reduces inter-slice signal leakage, which would present as "clusters" of false activation, between previously aliased voxel regions, as a result of correlation induced during aliased voxel separation.

2.2 Bootstrap sampling and artificial aliasing

To separate an aliased coil slice image, n_S bootstrap sampled coil slice images from the fully-sampled calibration slice images are averaged, then artificially aliased, and repeated for each time-point in the aliased slice image time-series. For a single time-point, a voxel in the same (x,y) location across the n_S slices measured at n_C coils, bootstrap sampled from the calibration slice image time-series, is represented in the $2n_Sn_C\times1$ vector, ν, and the mean bootstrap sample for each time point is represented in the $2n_Sn_C\times1$ vector, $\bar{\nu}$. The true mean voxel values, to be aliased in the same (x,y) location across the n_S slices, from the calibration slice images are represented by the $2n_S\times1$ vector μ, with the same voxel indices as in β for Eq. [2]. The vector, ν, has a $2n_Sn_C\times1$ error vector, η, with $\eta=(\eta'_R,\eta'_I)'$ corresponding to the real and imaginary parts of the measurement error of the coil calibration slice images for n_S slices measured at n_C coils. The calibration slice coil images measurement error has a mean of $E(\eta)=0$, and a covariance of

$$\mathrm{cov}(\eta)=\sigma^2 I_{2n_Cn_S}. \quad [6]$$

In the mSPECS model, for the δ^{th} aliasing pattern, the mean calibration images, $\bar{\nu}$, are artificially aliased with the $2n_C(n_S-1)\times2n_Sn_C$ aliasing matrix C_δ, which is the Kronecker product of the +1 and -1 Hadamard coefficients and vectors of ones, is

$$C_\delta = \mathbf{1}_{n_C} \otimes [\bar{H}_{\delta,1} \otimes \mathbf{1}_2,\ldots, \bar{H}_{\delta,n_S} \otimes \mathbf{1}_2].$$

The $(n_S-1)\times n_S$ matrix $\bar{H}_\delta$ is the remaining $(n_S-1)\times n_S$ matrix with the δ^{th} acquisition removed from the H matrix, so that C_δ is the remaining (n_S-1) orthogonal ways the true fully acquired voxels across the n_S slices could be aliased with a Hadamard matrix. An illustration of the origin of $\bar{H}_\delta$ to create the potential aliasing matrices, C_δ, for the n_S aliasing patterns, is shown in Fig. 2 for a Hadamard encoded time-series with $n_S=4$ aliased slice images. Fig. 2a is the time-series aliasing pattern that repeats every n_S TRs, denoted by the gray dashed line in the figure. The first 4 TRs

correspond to Hadamard aliasing of the four aliased slice images shown in Fig. 2b, with the four aliasing patterns shown as the sum and difference of the individual slice images. Fig. 2c is an illustration of the bootstrap sampling and artificial aliasing algorithm, and Fig. 2d depicts the four artificial aliasing matrices for MB4 for the δ^{th} aliasing pattern equivalent to the δ^{th} row of a Hadamard matrix of dimension $n_S \times n_S$ where $\delta = 1 \ldots . n_S$, and the gray shaded region designated the n_S-1 ways to artificially alias the calibration slice images corresponding to the δ^{th} aliasing pattern.

*** Fig. 2 appears near here***

To incorporate n_α subsequent TRs from the aliased voxel acquisition, the corresponding aliasing matrices, C_δ, are placed along the diagonal to create a single aliasing matrix C, of dimension $2n_C n_\alpha(n_S\text{-}1) \times 2n_S n_C n_\alpha$,

$$C = \begin{bmatrix} C_1 & & 0 \\ & \ddots & \\ 0 & & C_{n_\alpha} \end{bmatrix}. \quad [7]$$

Artificially aliasing the mean bootstrap sampled voxels, $\bar{v}$, and the corresponding error vector, η, from the calibration images with the aliasing matrix in Eq. [7] results in a $2n_\alpha n_C(n_S\text{-}1) \times 1$ vector,

$$\upsilon = C\bar{v} = C_A\mu + C\eta, \quad [8]$$

where μ has been previously defined as the $2n_S \times 1$ vector of the true calibration voxel values with real and imaginary parts. The matrix C_A is a coil sensitivity matrix with Hadamard coefficients, analogous to $(X_A)_\delta$, for the artificially aliased calibration voxels is the $2n_C(n_S\text{-}1) \times 2n_S$ matrix,

$$(C_A)_\delta = \left[\bar{H}_{\delta,1} \otimes \begin{pmatrix} S_{1,1} \\ \vdots \\ S_{n_C,1} \end{pmatrix}, \ldots, \bar{H}_{\delta,n_S} \otimes \begin{pmatrix} S_{1,n_S} \\ \vdots \\ S_{n_C,n_S} \end{pmatrix} \right].$$

Similar to Eq. [4], $(C_A)_\delta$ is generalized to C_A, of dimension $2n_\alpha n_C(n_S\text{-}1) \times 2n_S$, for the incorporation of n_α sequential TRs in the aliased voxel separation,

$C_A = [(C_A)_1, \ldots, (C_A)_{n_\alpha}]'$.

2.3 A separation of aliased voxel values

With the mSPECS approach, to separate the aliased voxel values, Eq. [2] and Eq. [8] are concatenated into one equation,

$$\begin{bmatrix} a \\ \upsilon \end{bmatrix} = \begin{bmatrix} X_A\beta \\ C_A\mu \end{bmatrix} + \begin{bmatrix} \varepsilon \\ C\eta \end{bmatrix}. \quad [9]$$

If y_a is the $2n_\alpha n_S n_C \times 1$ vector of acquired aliased voxel values stacked over the artificially aliased voxel values such that $y_a = (a', \upsilon')'$, and X is the two aliasing matrices concatenated, $X = [X_A', C_A']'$ of dimension $2n_\alpha n_S n_C \times 2n_S$, then the separation of the aliased voxel values in Eq. [9] is a least squares estimate of the form

$\hat{\beta} = (X'X)^{-1}X'y_a$,

The $2n_S \times 1$ vector of estimated separated voxel values with real and imaginary parts, is also written

$\hat{\beta} = (X'_A X_A + C'_A C_A)^{-1}(X'_A a + C'_A \upsilon)$

To view the mSPECS approach as a Bayesian method, where $a \sim N(\beta, \sigma^2 I_{2n_c n_\alpha})$ and $\bar{v} \sim N(\mu, \sigma^2 I_{2n_c n_\alpha n_S})$, so the posterior mean is

$E[\hat{\beta}] = (X'_A X_A + C'_A C_A)^{-1}(X'_A \beta + C'_A \mu)$,

such that the separated voxel values are a weighted combination of prior and likelihood mean voxel values, or calibration and artificially aliased true voxel values.

The covariance of the added measurement error of a measured aliased voxel in Eq. [2] measured at n_C coils, which is n_α sequential TRs incorporated into mSPECS,

$\text{cov}(\varepsilon) = \sigma^2 I_{2n_c n_\alpha}$

[10]

and the covariance of the artificially aliased n_S calibration voxel values measured at n_C coils, which is n_α sequential TRs in Eq. [8] is

$\text{cov}(C\eta) = \sigma^2 I_{2n_c n_\alpha (n_S - 1)}$.

[11]

In both Eq. [10] and Eq. [11], there is no covariance between the real and imaginary parts, and a constant variance of σ^2 for both real and imaginary parts. The $2n_\alpha n_C n_S \times 2n_\alpha n_C n_S$ covariance matrix for the $2n_\alpha n_C n_S \times 1$ vector y_a, consisting of aliased and artificially aliased voxel values is

$$\text{cov}(y_a) = \begin{bmatrix} \sigma^2 I_{2n_\alpha n_C} & 0 \\ 0 & \tau^2 I_{2n_\alpha n_C (n_S - 1)} \end{bmatrix}. \quad [12]$$

If there is no variation, i.e. no random sampling of the calibration voxel values with mSPECS, among the average calibration slice images used to separate each aliased image then $\tau^2 = 0$. The

bootstrapping adaptation averages n_S randomly selected calibration images for each TR in $\bar{v}_j$ to obtain $\tau^2 = \sigma^2$, such that the covariance in Eq. [12] results in the $2n_S \times 2n_S$ matrix,

$\text{cov}(\hat{\beta}) = \sigma^2 (X_A' X_A + C_A' C_A)^{-1}$.

The inclusion of the calibration images through the mSPECS method reduces correlation between the previously voxel values, compared to Eq. [5], since $C_A' C_A$ acts as a regularizer, which improves the condition of Eq. [9]. In SMS-fMRI, induced correlation from the un-aliasing of the slice images throughout the time-series, presents as inter-slice signal leakage among previously aliased voxels, with false activation detected in these regions (8).

3. Methods and materials

The mSPECS method is demonstrated with Hadamard encoded simulated phantom and experimental human data. With Hadamard matrix dimensions increasing in powers of two, the design of task timings also increases in powers of two to accommodate various accelerations determined post acquisition, by varying n_α in the mSPECS method. The data is acquired with a MB factor of 8, with an 8 second TR and no acceleration. The TR is based from the timing of full volume acquisitions, so 9 packets of 8 aliased slices are measured yielding 72 slices in 8 seconds with no acceleration. The net acceleration after slice separation is defined as the number of aliased slices divided by the number of sequential TRs utilized in the reconstruction, $A = n_S / n_\alpha$. The notation "mSPECS 2" denotes an implementation of mSPECS with A=2. The number of sequential TRs used for reconstruction changes the TR length, from TR_{acq} (the acquired TR length as defined in Fig. 1) to TR_{sep} (the TR length of the separated slice image time-series) with $\text{TR}_{\text{sep}} = \text{TR}_{\text{acq}} n_\alpha$.

The total time of the time-series remains the same, although the number of time points differs before and after slice separation, where the time-points post slice image separation is equivalent to the starting number of TRs divided by n_α.

3.1 Phantom Simulation

An fMRI digital phantom (19, 20) data set was generated with a block-design of task activity, with an initial rest of 64 seconds followed by 9 epochs of 32 seconds no task and 32 seconds task using MATLAB (The Mathworks, Natick, MA, USA). The data was generated for eight sagittal slice images that are 96×96 in dimension to represent one packet in a full brain volume

Hadamard encoded acquisition. The noiseless time series was generated for each slice image with a theoretical T_2^* weighted phantom with initial values between 0 and 1, then weighted for maximum SNR of 30 in the magnitude, yielding an approximate SNR of 30 in the CSF, 15 in the grey matter, and 7 in the white matter, and a mean phase is added to the slice images varied from $8\pi/36$ to $\pi/36$ from slice one to slice eight decreasing in increments of $\pi/36$. The calibration time-series was generated with 40 TRs from the complex-valued phantom. The slices are first weighted by complex-valued simulated 16-channel coil sensitivity maps, then standard Gaussian noise was added to the real and imaginary components of the time series. The simulated coil profiles were generated with a bivariate normal probability density function with mean 0 and with a covariance matrix $\sigma^2 I_2$,where $\sigma^2=96/2$, and the first 4 coils are placed in the four corners and the next 4 coils on the four edges, then repeated for a total of 16 receive coils. Sixteen weighting matrices, with values between 0 and 1, are generated, rotated for each slice, and applied to the coil profiles, such that each slice has a unique weighting of the 16-channel coil profiles. For the complex-valued coil profiles, a phase of $\pi/12$ is added to each coil profile.

In the simulation, the task was generated in one unique 6×6 voxel square region of interest (ROI) placed in a clockwise rotation for each slice with a magnitude contrast-to-noise ratio (CNR) of 0.5. For a magnitude CNR of 0.5, the magnitude within the ROI is increased by 0.5 for 32 TRs and then returning to baseline for the following 32 TRs for the 9 epochs. Before the complex-valued time-series was summed in the slice direction, the Hadamard phase encoding was simulated. With no in-plane parallel imaging acceleration, i.e. mSPECS, the Hadamard pattern resembled in Fig. 2, depending on the number of aliased slices or multiband factor. Once the complex-valued slices are multiplied by the +1 or -1 Hadamard phase encode coefficient, they weighted by the complex-valued 16-channel coil sensitivities, then summed in the slice direction. Standard Gaussian noise was added to the real and imaginary components of the time series. One time-series of Hadamard aliased images, simulated with MB8, was then separated using the mSPECS model and separated with n_α=1, 2, 4, and 8, or equivalently written as mSPECS 1, mSPECS 2, mSPECS 4, mSPECS 8, and fMRI activation was calculated in each separated voxel using a complex-valued fMRI model (11), and the region outside the brain is masked.

3.2 Experimental Human Subject Data

An experimental fMRI human data set with Hadamard encoding was acquired with a visual flashing checkerboard stimulus presented in a block design with an initial 64 seconds rest followed by 9 epochs of 32 seconds on and 32 seconds off using a 3.0 T Discovery MR750 MRI scanner (General Electric, Milwaukee, WI) with a 32-channel receive coil. The data was acquired with nine interleaved sagittal packets that are 96×96 in dimension and 2 mm thick. Eight Hadamard encoded slices are simultaneously magnetized within each slice packet, for a total of 72 slice images after slice image separation. The imaging parameters included a 24.0 cm FOV, a TR/TE of 1000/41 ms, a flip angle of 11°, an acquisition bandwidth of 250 kHz, and an effective echo spacing of 0.500 ms. The calibration non-task fMRI human data set without Hadamard encoding, was also acquired with 72 sagittal slices that are 96×96 in dimension and 2 mm thick. The imaging parameters included a 24.0 cm FOV, a TR/TE of 8000/41 ms, a flip angle of 11°, an acquisition bandwidth of 250 kHz, and an effective echo spacing of 0.500 ms. The phase encoding direction was oriented as superior to inferior (bottom to top in images). The images were Nyquist ghost corrected (21), with the phase error averaged across each voxel time-series.

Before applying the mSPECS separation to the aliased slices, a phase correction is applied to the aliased time-series, and both a phase and magnitude correction is applied to the calibration images. First, each Hadamard pattern in the aliasing phase time-series is corrected. The mean phase of each Hadamard pattern is estimated, and then subtracted from the phase time-series of the corresponding pattern. The residual images of the phase time-series are fit to a local third order polynomial, with a local fit region of 11×11 voxels, the fit subtracted, and the mean phase image is added back to the phase time-series. Second, the full complex-valued Hadamard aliased time-series is separated with addition and subtraction, and the mean phase of the separated slice time-series is estimated. The calibration image phase time-series is also corrected in the same way. The mean phase of the slice time-series is estimated, and then subtracted from the phase time-series. The residual images of the phase time-series is again fit to a local third order polynomial, with a local fit region of 11×11 voxels, the fit subtracted, and the mean phase estimated from the Hadamard separated images is added back to the calibration time-series. The difference in magnitude between the voxels in the calibration coil images and Hadamard coil image time-series is reconciled by multiplying the magnitude calibration images with a magnitude difference ratio of 0.2. The magnitude difference ratio is the mean magnitude

Hadamard separated images at each coil divided by the mean magnitude calibration images at each coil, with the regions of signal dropout masked in the Hadamard separation for the estimation of the ratio.

The raw 32-channel receive coil sensitivity maps are estimated from the calibration slice images. The complex-valued coil sensitivity profiles are estimated by averaging the time-series for each coil slice image. The mean coil slice images are normalized, by averaging along the coil dimension to form a single slice image, the sensitivity map, and the sensitivity maps are fit to a local polynomial, the local fit region is 13×13 voxels and the polynomial is of order three, to remove variability in the maps. The aliased images were then separated using the mSPECS model, and fMRI activation was calculated in each separated voxel using the complex-valued fMRI model in (11). The Hadamard aliased images, acquired with MB8, was then separated using the mSPECS model and separated with A=1, 2, 4, and 8, or equivalently written as mSPECS 1, mSPECS 2, mSPECS 4, mSPECS 8, the fMRI activation was calculated in each separated voxel using a complex-valued fMRI model (11), and the region outside the brain is masked.

4. Results

4.1 Simulation Results

The magnitude and phase of the time-series mean for the calibration slice images for the eight complex-valued aliased slice images for the digital phantom simulation are shown in Fig. 3a, the calibration slice images are measured with the simulated 16-channel receive coils and the fully sampled coil images are combined with a SENSE reconstruction. The magnitude and phase of the time-series mean for the Hadamard separated slice images for the eight complex-valued aliased slice images for the digital phantom simulation are shown in Fig. 3b, the aliased slice images are measured with the simulated 16-channel receive coils, separated with adding and subtracting the complex-valued images, and the separated slice coil images are combined with a SENSE reconstruction. In Fig. 4 and Fig. 5 are the calibration magnitude and phase slice images of the mean time-series separated for the reconstructions of mSPECS 1, mSPECS 2, mSPECS 4, and mSPECS 8. Across the four accelerations, in the mean separated slice magnitude and phase images, there are no signs of residual aliasing (slice leakage) induced from slice image separation.

After the mSPECS slice image separation of the aliased time-series, the activation statistics are calculated in each voxel using the complex-valued fMRI model in (11). The *z*-scores for the activation statistics are mapped in Fig. 6, and the regions where the activation was placed is highlighted by the green box in each slice. The z-score from the activation maps are thresholded at 2, and the region outside the digital phantom is masked. Since the activation is placed in a unique 6×6 region in each slice image, before simulating the aliased time-series, and there are no incremental shifts in the FOV, inter-slice signal leakage stemming from the slice separation process is easily identifiable by visually examining previously aliased voxel locations. The regions within the green boxes show strong activation clusters. The average *z*-scores increase as the acceleration increases, with the *z*-scores in mSPECS 4 and mSPECS 8 appear similar. A higher sampling rate corresponds to a strengthened statistical significance, although we expect the reduced acceleration images to have a higher SNR. The *z*-scores in mSPECS 2 are higher than mSPECS 1, yet the difference between the *z*-scores in mSPECS 2 versus mSPECS 4 or mSPECS 8 is not as large. There are no clusters of "active" voxels outside the green boxes in Fig. 6, so active voxels outside indicate false positives from noise in the time-series, rather than inter-slice signal leakage.

*** Fig. 3 appears near here***

*** Fig. 4 appears near here***

*** Fig. 5 appears near here***

*** Fig. 6 appears near here***

4.2 Human Subject Data Results

The magnitude and phase of the time-series mean for the calibration slice images for the eight complex-valued aliased slice images for the human subject are shown in Fig. 7a, the calibration slice images are measured with the 32-channel receive coils and the fully sampled coil images are combined with a SENSE reconstruction. The magnitude and phase of the time-

series mean for the Hadamard separated slice images for the eight complex-valued aliased slice images for the human subject are shown in Fig. 7b, the aliased slice images are measured with the 32-channel receive coils, separated with adding and subtracting the complex-valued images, and the separated slice coil images are combined with a SENSE reconstruction. In Fig. 8 and Fig. 9 are the magnitude and phase time-series mean of the slice images separated for the reconstructions of mSPECS 1, mSPECS 2, mSPECS 4, and mSPECS 8. In the four accelerations, there is signal dropout in the same locations for each slice image. The signal dropout regions in the magnitude in Fig. 8 correspond to the same regions seen in Fig. 7b. The mSPECS separation is susceptible to the same signal dropout observed in the addition and subtraction schemes. This signal dropout is a data quality issue, arising from potential complications with subject motion, rather than a direct result of the mSPECS separation itself. As acceleration increases, the mean magnitude images in Fig. 8 show less decreased signal attenuation. During acquisition, if there is a "poor" aliasing pattern throughout the time-series, i.e. the +/- orthogonality is not maintained during the slice excitations, the impact will lessen as acceleration increases with the mSPECS approach to aliased slice image separation.

After the mSPECS slice image separation of the aliased time-series, the fMRI activation statistics are calculated in each voxel using the complex-valued fMRI model in (11). The *z*-scores for the activation statistics are mapped in Fig. 10. The activation maps are thresholded at 1.5, and the region outside the brain is masked. While there does not appear to be signal leakage from the BOLD signal, the activation maps are noisy, which may be potentially structured noise as a result of subject motion. Slice 6 shows the most well defined region of activation in the visual cortex, this finding corroborates the signal dropout observed in the magnitude images in Fig. 8. Note, the data has been minimally processed, to prevent processing induced correlations presenting in the separated slice image time-series. The activation observed within the frontal lobe, may be attributed to subject motion with respect to the flashing checkerboard stimulus.

*** Fig. 7 appears near here***

*** Fig. 8 appears near here***

*** Fig. 9 appears near here***

*** Fig. 10 appears near here***

5. Discussion and Conclusions

Without whole brain volume fMRI-SMS acquisitions and separation methods, either spatial or temporal resolution is constrained during experimental data acquisition. Although, many SMS reconstruction techniques ignore the statistical implications of fast imaging methods on the fMRI time-series analysis. The implementation of the mSPECS separation in simulation yields very promising results. In simulation, the activation in each slice is accurately placed and there is no task signal leakage between previously aliased voxels. Increasing the acceleration yields a higher sample size and improves the statistical significance of the data, so larger *z*-scores are observed as the acceleration increases, with the most substantial gains observed the *z*-scores between the reconstructions of mSPECS 1 and mSPECS 2. The development of complex-valued SMS reconstruction methods allows for increased statistical significance from a higher sampling rate of time points, and complex-valued fMRI analysis which has been shown to improve fMRI activation statistics.

The benefits of an implementation of the mSPECS separation in an acquisition of a Hadamard encoded fMRI time-series is less straightforward than observed in simulation. The quality of the mSPECS slice separation is dependent on the acquisition, and Hadamard addition and subtraction schemes are susceptible to signal dropout from subject motion or potentially from non-orthogonal phase encoding arising from magnetic field inhomogeneities. Subject motion will negatively impact the mSPECS reconstruction in two ways. First, with motion between the calibration images and the Hadamard encoded images, the mean voxel values between the two sets of images will not align, yielding a poor least squares separation. This is a draw back with mSPECS and any SMS reconstruction method. Second, subject motion during the Hadamard scan results in spin history artifacts, which will destructively interfere with the reconstruction, as the signal intensity of the aliased slices will not be uniform across the time-series. The spin history artifacts may also occur from subject motion during the slice acquisition or between sequential slice acquisitions, which will also impact the manifestation of the artifact,

and make it difficult to identify the origin of the artifact. The issue with motion and spin history are particularly sensitive in Hadamard schemes, with add and subtract nature of the separation, compared to other SMS reconstruction methods. Problems also arise with the aliased slice separation when the orthogonal encoding is not perfectly orthogonal. The mSPECS separated slice images from the human experimental data also present artifacts arising in the separated magnitude images from phase transitions between voxels.

An application of the mSPECS reconstruction, to a blipped-CAIPI acquisition, rather than Hadamard encoded acquisitions, is a future addition to this research. The mSPECS methods easy facilitates the blipped-CAIPI acquisitions by changing the Hadamard aliasing matrices to reflect the shifted FOV aliasing patterns associated with blipped-CAIPI acquisitions. There are potential difficulties associated with blipped-CAIPI acquisitions, such as disentangling the signal of interest from the ghosting artifacts in the reconstructed images. A comparison of mSPECS to the Split Slice GRAPPA (7) reconstruction, using the same blipped-CAIPI acquisition is also of interest for future research.

Acknowledgements

This work was supported by NIH NS087450 and NSF DMS-1127914.

References

1. Sodickson DK, Manning WJ. Simultaneous Acquisition of Spatial Harmonics (SMASH): Fast Imaging with Radiofrequency Coil Arrays. Magn Reson Med 1997;4:591–603.
2. Pruessmann KP, Weiger M, Scheidegger MB, Boesiger P. SENSE: Sensitivity Encoding for fast MRI. Magn Reson Med 1999;42:952–962.
3. Griswold MA, Jakob PM, Heidemann RM, Nittka M, Jellus V, Wang J, Kiefer B, Haase A. Generalized Autocalibrating Partially Parallel Acquisitions (GRAPPA). Magn Reson Med 2002;47:1202–1210.
4. Larkman DJ, Hajnal JV, Herlihy AH, Coutts GA, Young IR, Ehnholm G. Use of multicoil arrays for separation of signal from multiple slices simultaneously excited. Magn Reson Imag 2001;13:313–317.
5. Setsompop K, Cauley SF, Bhat H, Polimeni J, Wald LL. Characterization and Mitigation of Signal Leakage in Simultaneous Multi-Slice (SMS) Acquisition. Proc Intl Soc Magn Reson Med 2013;21:3315.
6. Moeller S, Xu J, Auerbach EJ, Yacoub E, Ugurbil K. Signal leakage (*l*-factor) as a measure of parallel imaging performance among simultaneously multislice (SMS) excited and acquired signals. Proc Intl Soc Magn Reson Med 2012;20:519.
7. Cauley SF, Polimeni J, Bhat H, Wald LL, Setsompop K. Interslice Leakage Artifact Reduction Technique for Simultaneous Multislice Acquisitions. Magn Reson Med 2014;72:93–102.

8. Todd N, Moeller S, Auerbach EJ, Yacoub E, Flandin G, Weiskopf N. Evaluation of 2D multiband EPI imaging for high resolution, whole brain task-based fMRI studies at 3T: Sensitivity and slice leakage artifacts. NeuroImage 2016;124:32–42.
9. Muller S. Multifrequency selective RF pulses for multislice MR imaging. Magn Reson Med 1998;6:364–371.
10. Souza SP, Szumowski J, Dumoulin CL, Plewes DP, Glover G. SIMA: simultaneous multislice acquisition of MR images by Hadamard-encoded excitation. Comput Assist Tomogr 1988;12:1026–1030.
11. Rowe DB, Logan BR. A complex way to compute fMRI activation. Neuroimage 2004; 23:1078–1092.
12. Rowe DB. Modeling both the magnitude and phase of complex-valued fMRI data, Neuroimage 2005;25:1310–1324.
13. Rowe DB. Magnitude and phase signal detection in complex-valued fMRI data. Magn Reson Med 2009;62:1356–1357.
14. Arja SK, Feng Z, Chen Z, Caprihan A, Kiehl KA, Adali T, Calhoun VD. Changes in fMRI magnitude data and phase data observed in block-design and event-related tasks, Neuroimage 2010;49:3149–3160.
15. Kociuba MK, Rowe DB. Complex-Valued Time-Series Correlation Increases Sensitivity in FMRI Analysis. Magn Reson Imaging. 2016;34:765–770.
16. Blaimer M, Choli M, Jakob PM, Griswold MA, Breuer FA. Multiband Phase Constrained Parallel MRI. Magn Reson Med 2013;69:974–980.
17. Blaimer M, Gutberlet M, Kellman P, Bruer FA, Kostler H, Griswold MA. Virtual Coil Concept for Improved Parallel MRI Employing Conjugate Symmetric Signals. Magn Reson Med 2009;61:93–102.
18. Sylvester JJ. Thoughts on Orthogonal Matrices, Simultaneous Sign-Successions, and Tessellated Pavements in Two or More Colours, with Applications to Newton's Rule, Ornamental Tile-Work, and the Theory of Numbers. Phil Mag 1867;34,461–475.
19. Karaman MM, Bruce IP, Rowe DB. Incorporating relaxivities to more accurately reconstruct MR images. Magn Reson Imaging 2015;33:85–96.
20. Rowe DB, Bruce IP, Nencka AS, Hyde JS, Kociuba MC: Separation of Parallel Encoded Complex-valued Slices (SPECS) from a Single Complex-valued Aliased Image. Magn Reson Imaging, 2016;34:359–369.
21. Nencka AS, Hahn AD, Rowe DB. The use of three navigator echoes in Cartesian EPI reconstruction reduces Nyquist ghosting. Proc Intl Soc Magn Reson Med 2008;16:3032.

Figure Legends

Figure 1: Slice profiles for a Hadamard encoded acquisition of $A = n_S = 2$ aliased slice images in 2 packets for a total of 4 slice images.

Figure 2: (a) The rotating Hadamard encodes to alias n_S=4 slice images (column) for n time-points (row), repeated every n_S TRs, denoted by the gray dotted line, (b) n_S=4 aliased slice images acquired over 4 consecutive time repetitions are the sum and difference of the individual complex-valued slice images, (c) the algorithm for the bootstrap sampling of calibration images, and (d) the corresponding artificial aliasing matrices, $\bar{H}$, for the δ^{th} aliasing pattern.

Figure 3: (a) Mean calibration digital phantom magnitude slice images and phase slice images, with the numbering 1 through 8 referring to the slice image number, and the (b) mean Hadamard separated digital phantom magnitude slice images and phase slice images, with the numbering 1 through 8 referring to the slice image number.

Figure 4: Mean magnitude mSPECS separated slice images from the Hadamard encoded digital phantom simulation for the accelerations of mSPECS 1, mSPECS 2, mSPECS 4, and mSPECS 8.

Figure 5: Mean phase mSPECS separated slice images from the Hadamard encoded digital phantom simulation for the accelerations of mSPECS 1, mSPECS 2, mSPECS 4, and mSPECS 8.

Figure 6: Activation statistics for the mSPECS separated slice images from digital phantom simulation for the accelerations of mSPECS 1, mSPECS 2, mSPECS 4, and mSPECS 8.

Figure 7: (a) Mean calibration magnitude slice images and phase slice images, with the numbering 1 through 8 referring to the slice image number, and the (b) mean Hadamard separated magnitude slice images and phase slice images, with the numbering 1 through 8 referring to the slice image number.

Figure 8: Mean magnitude mSPECS separated slice images from the Hadamard encoded human subject data for the accelerations of mSPECS 1, mSPECS 2, mSPECS 4, and mSPECS 8.

Figure 9: Mean phase mSPECS separated slice images from the Hadamard encoded human subject data for the accelerations of mSPECS 1, mSPECS 2, mSPECS 4, and mSPECS 8.

Figure 10: Activation statistics for the mSPECS separated slice images from the Hadamard encoded human subject data for the accelerations of mSPECS 1, mSPECS 2, mSPECS 4, and mSPECS 8.

Figure 1

Click here to download high resolution image

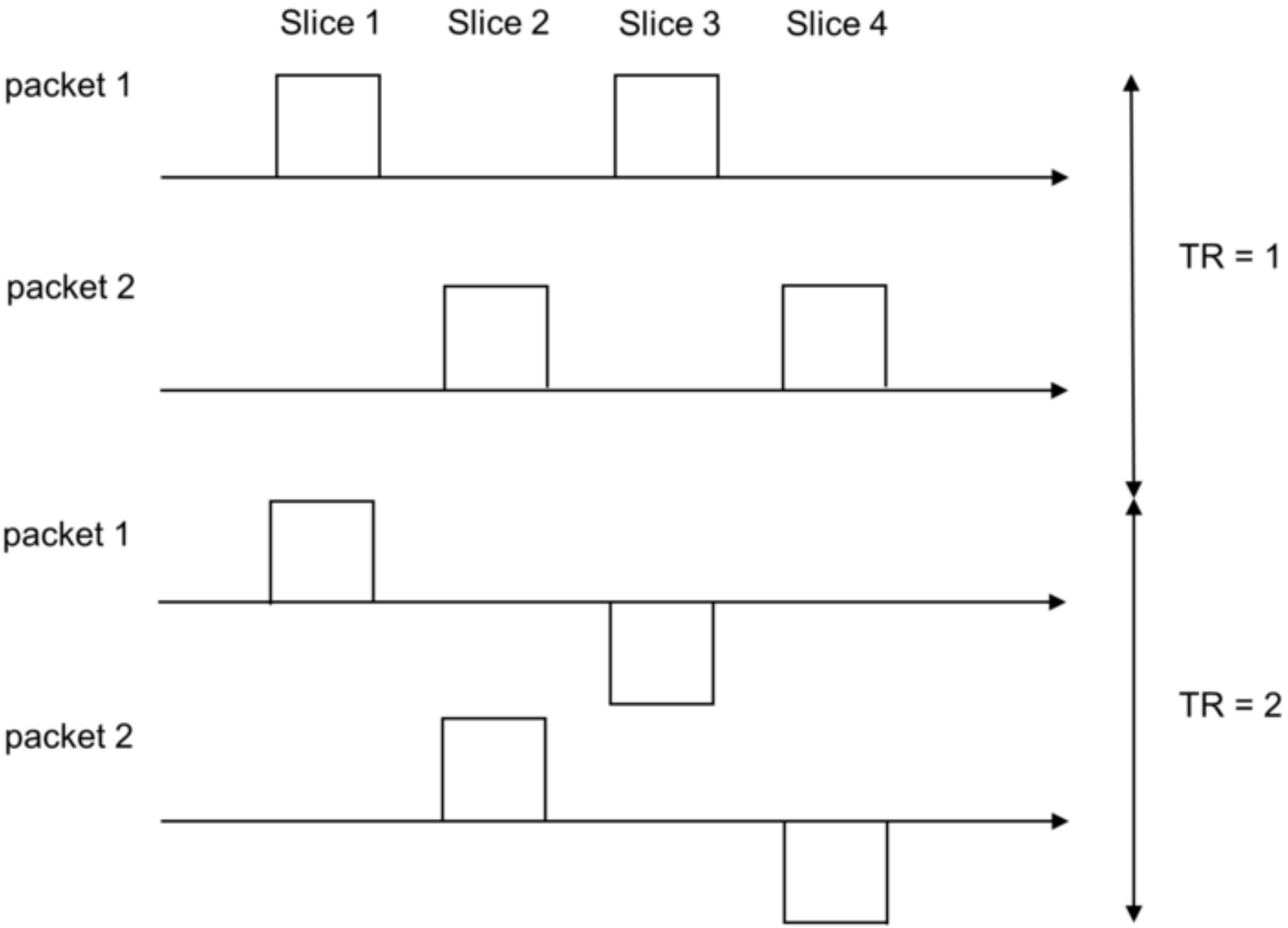

Figure 2

Click here to download high resolution image

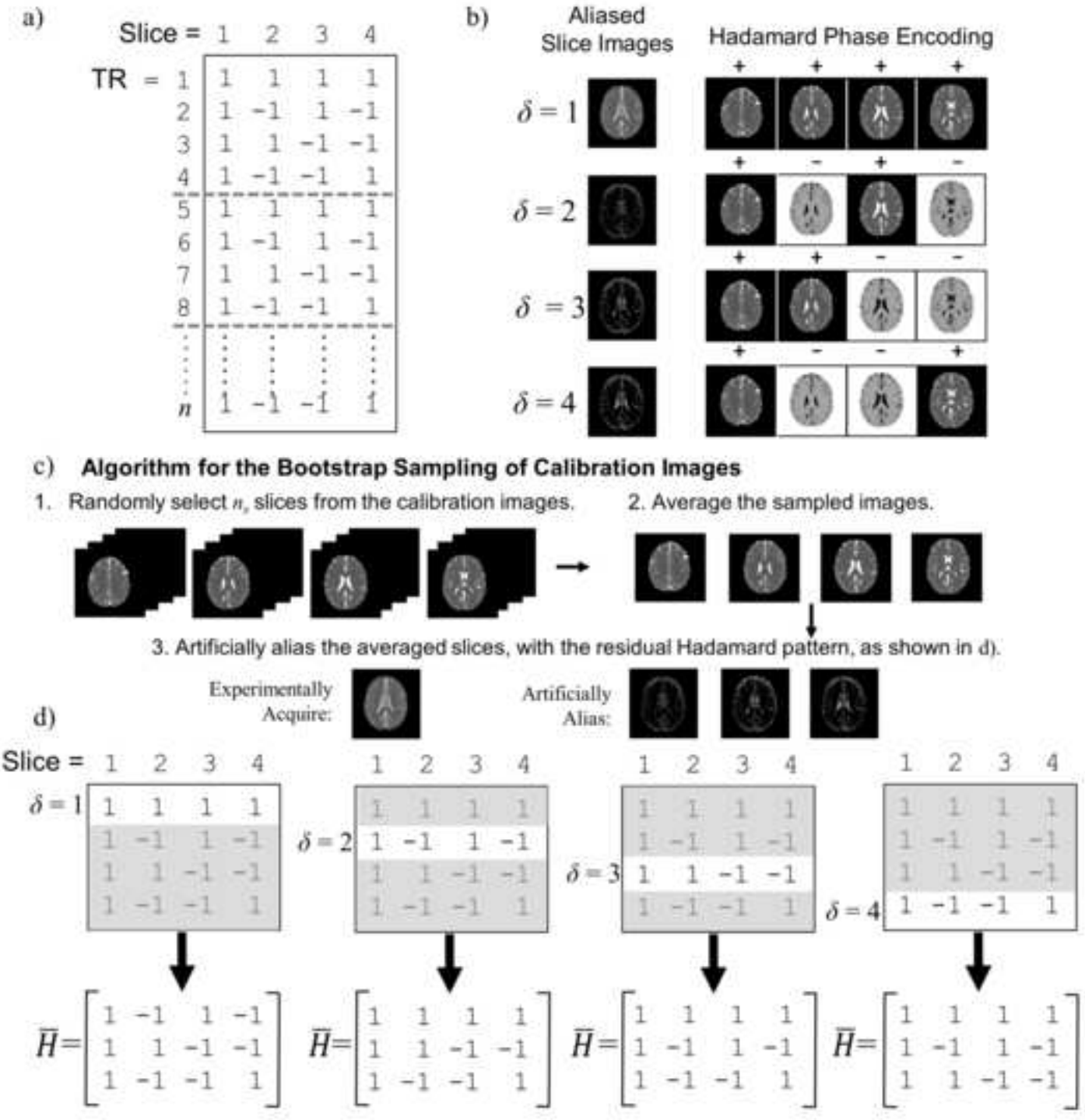

Figure 3

Click here to download high resolution image

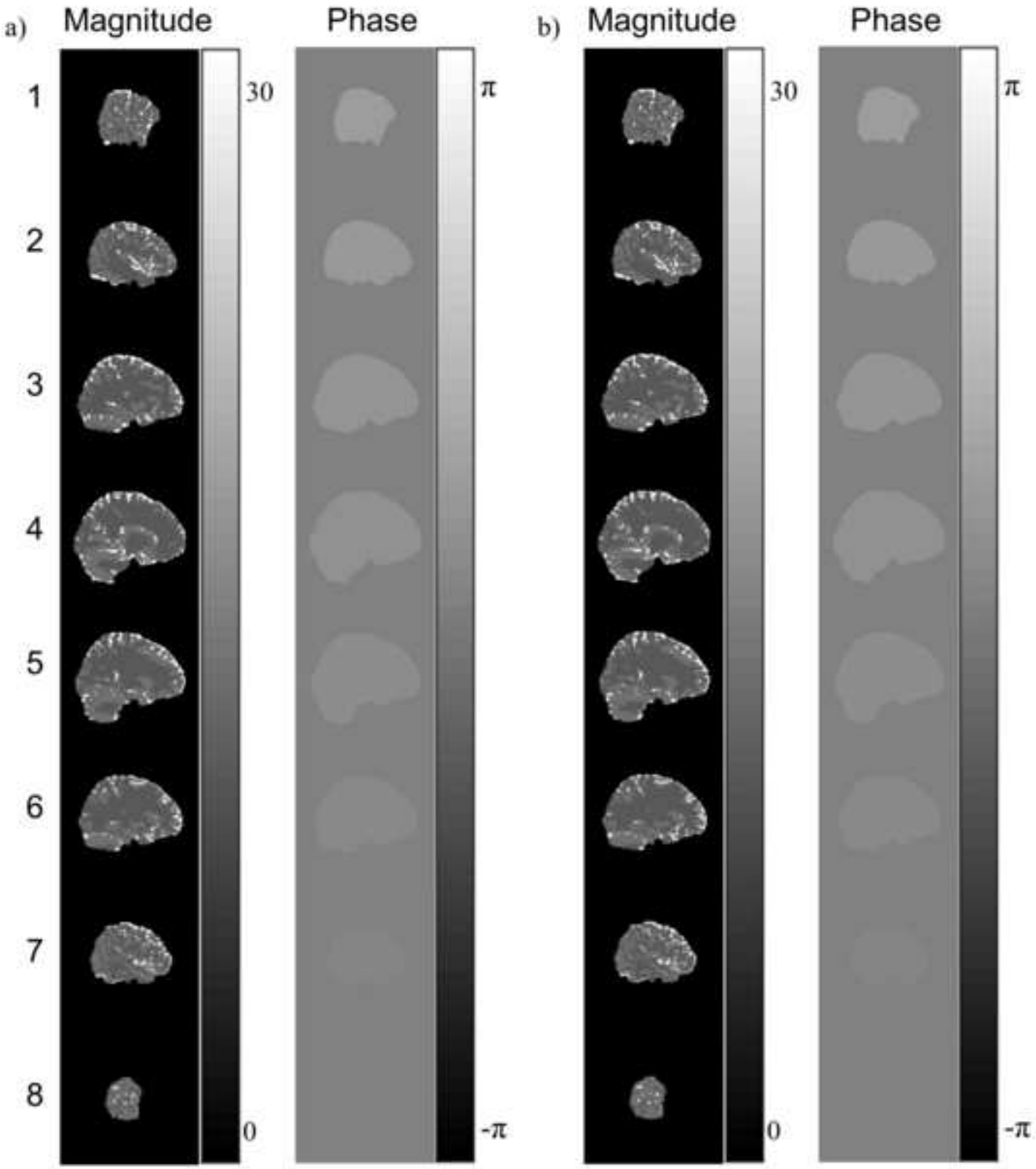

Figure 4

Click here to download high resolution image

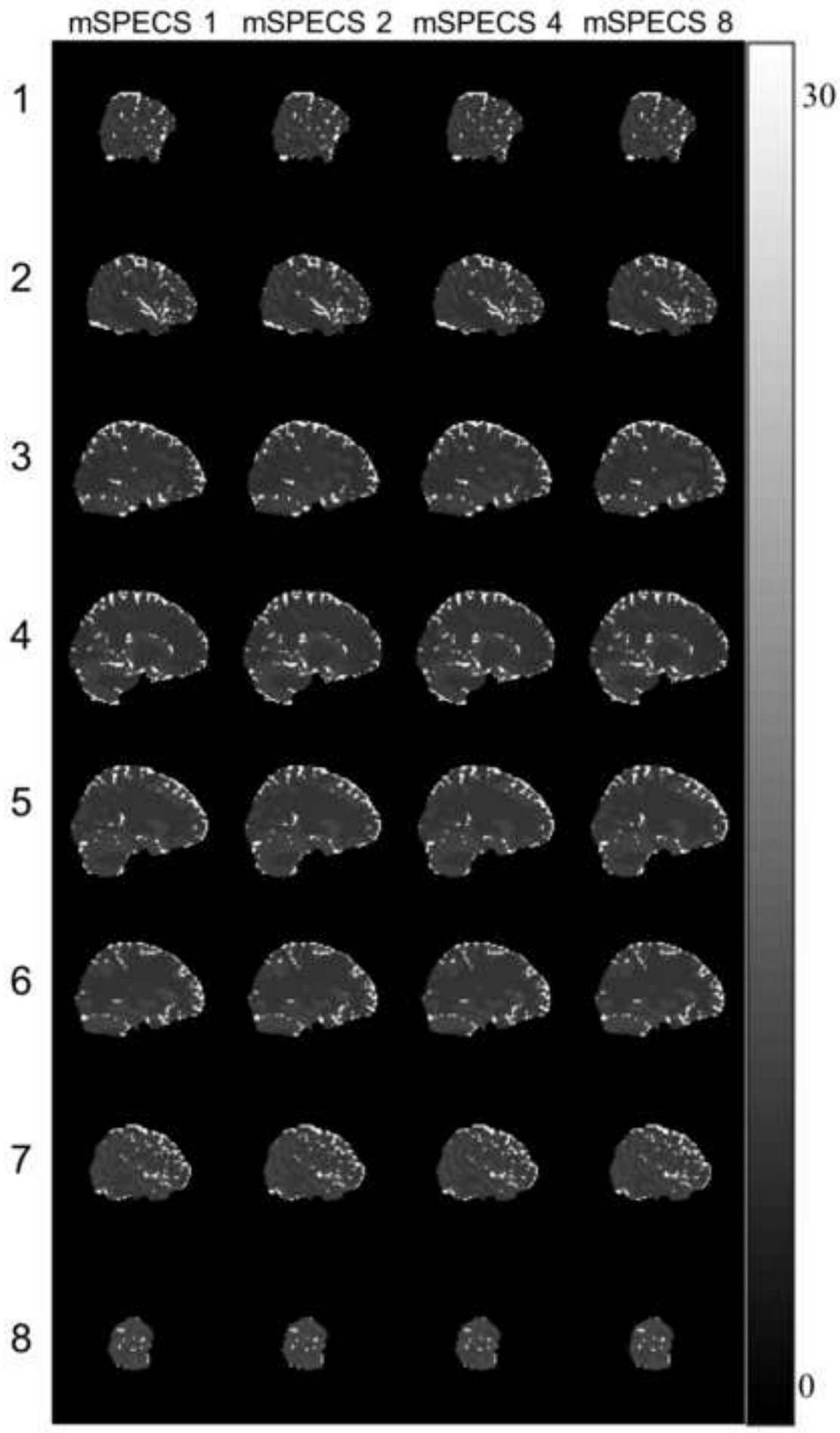

Figure 5

Click here to download high resolution image

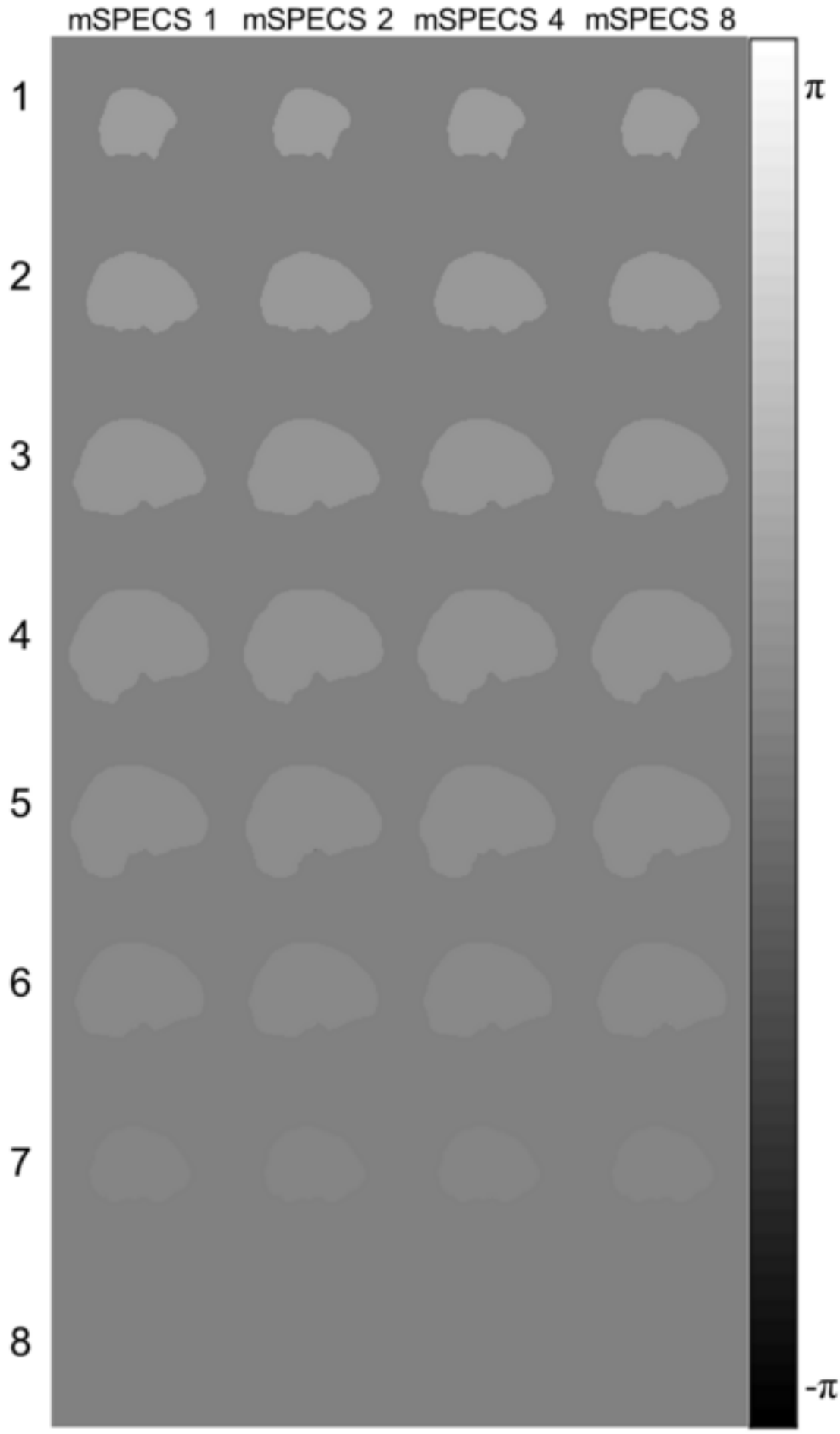

Figure 6

Click here to download high resolution image

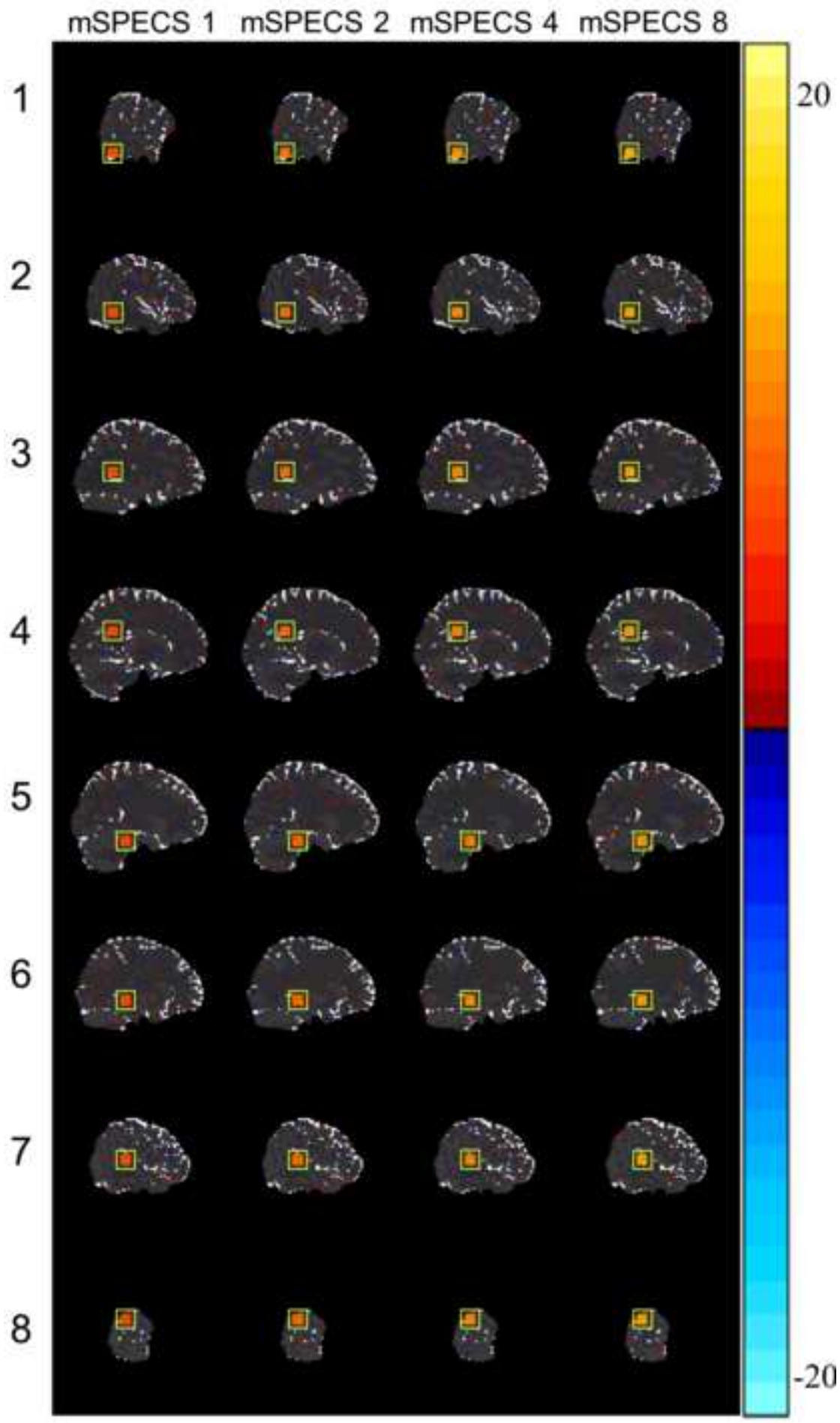

Figure 7

Click here to download high resolution image

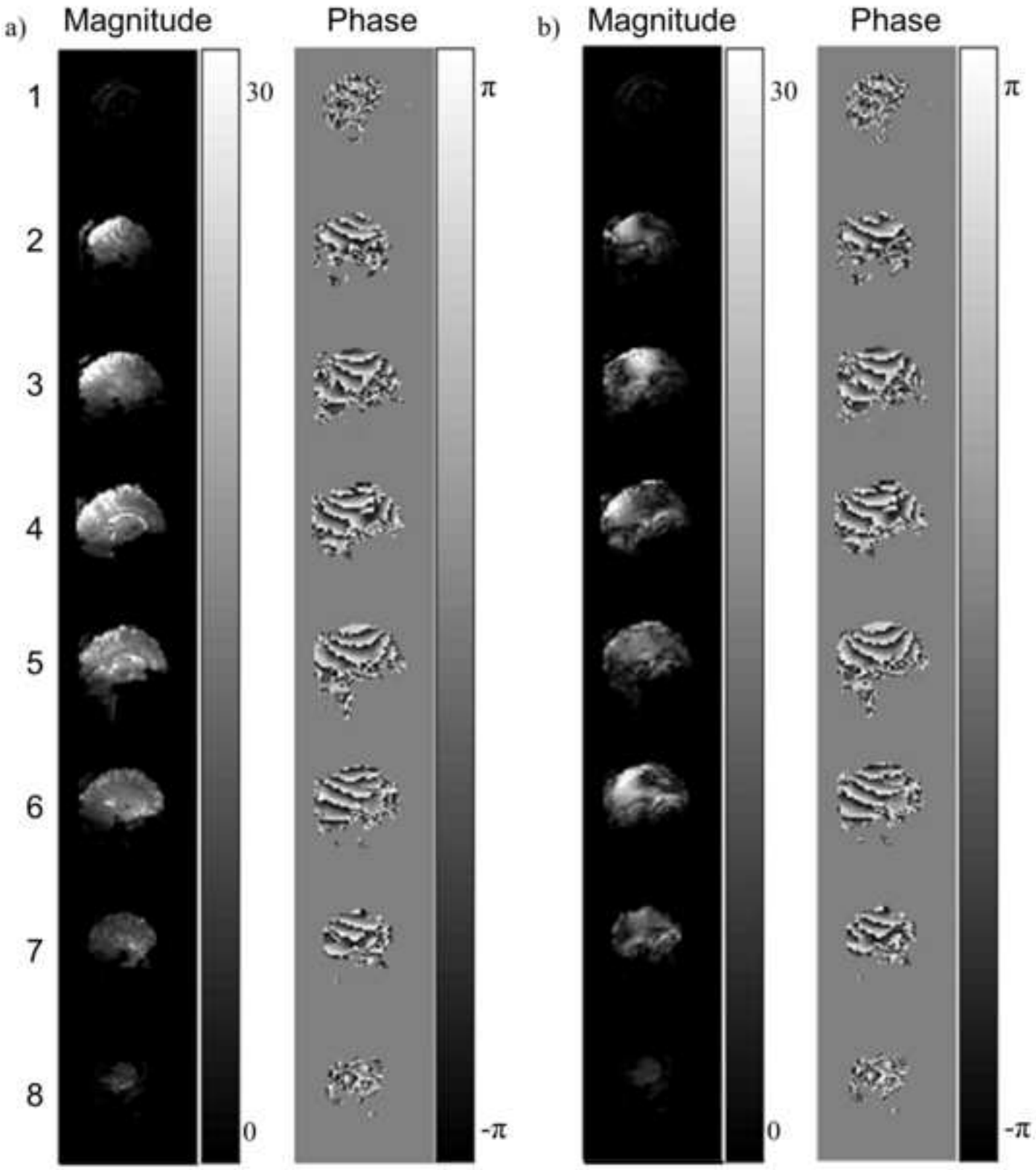

Figure 8

Click here to download high resolution image

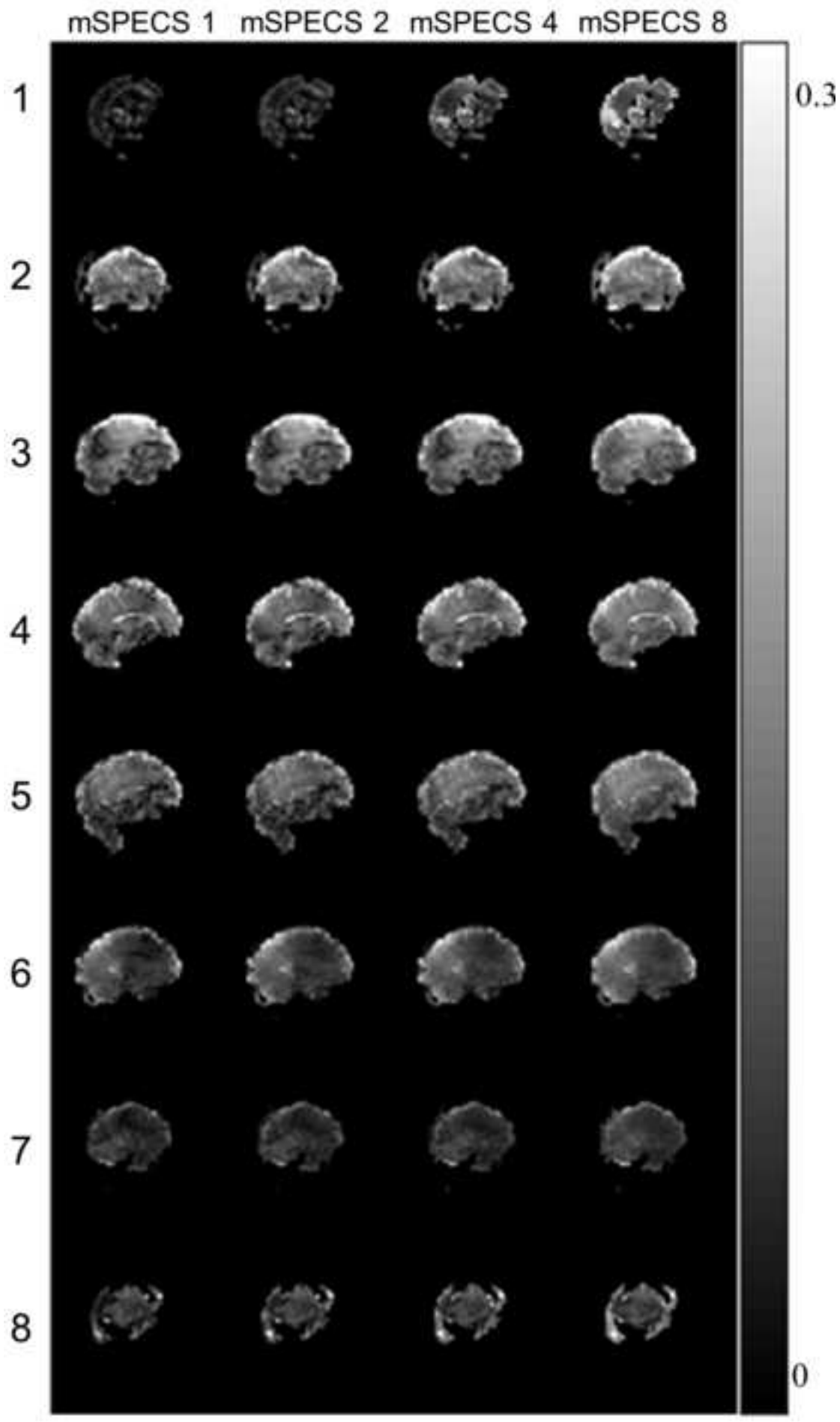

Figure 9

Click here to download high resolution image

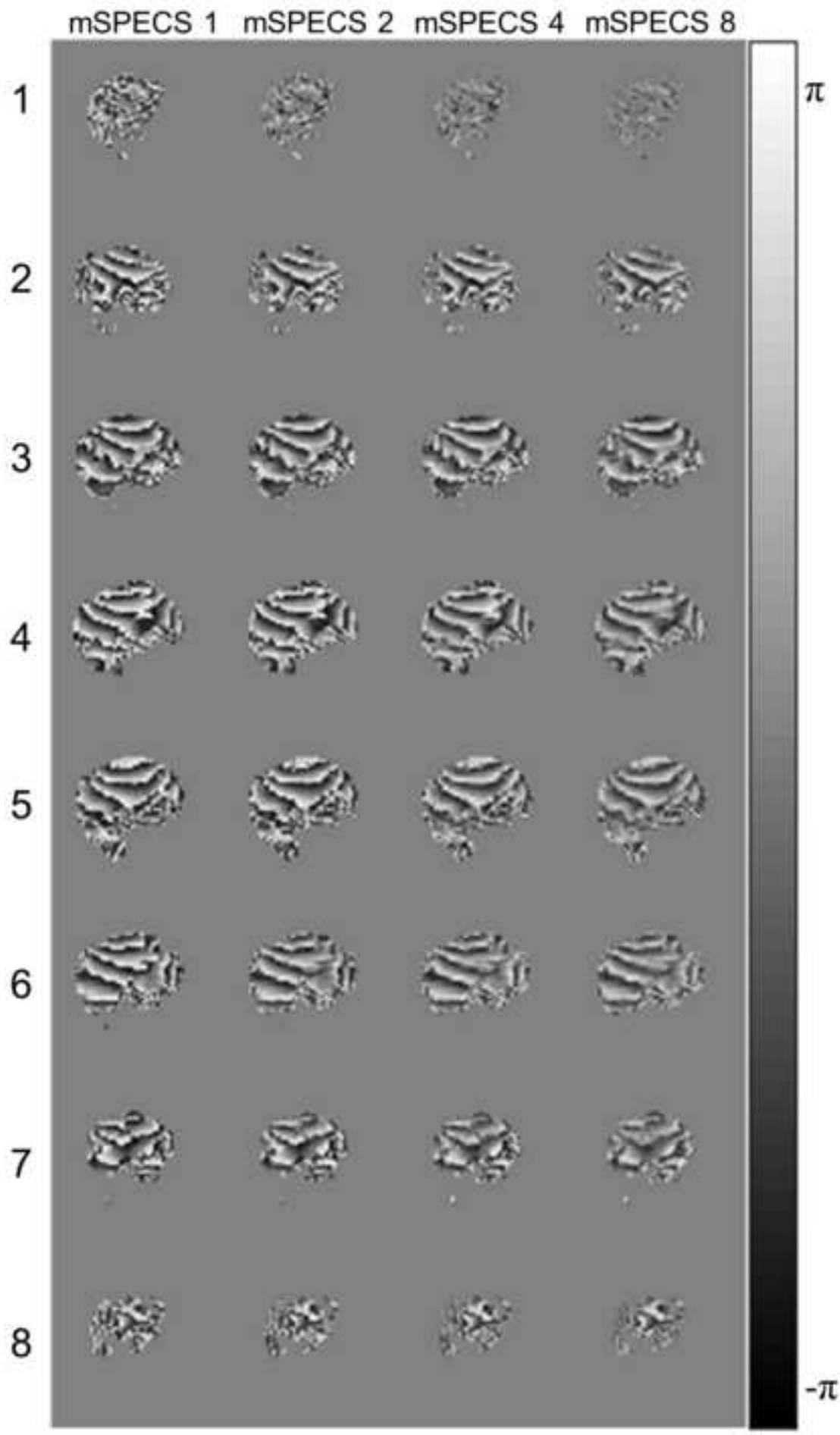

Figure 10

Click here to download high resolution image